Resonance Raman Spectra and Excited-State Structure of Aggregated Tetrakis(4-sulfonatophenyl)porphyrin Diacid

Dong-Ming Chen, Tianjing He, Di-Fei Cong, Ying-Hui Zhang, and Fan-Chen Liu*

Department of Chemical Physics, University of Science and Technology of China, Hefei, Anhui 230026, China

Received: September 18, 2000; In Final Form: January 25, 2001

Resonance Raman (RR) spectra of aggregates of tetrakis(4-sulfonatophenyl)porphyrin diacid (H_4TSPP^{2-}) excited near exciton absorption bands of 489 nm (J_B band) and 421 nm (H_B band) were recorded and analyzed, and RR intensities of the aggregates and segregated monomers were calculated with time-dependent resonant Raman formulas for the Franck−Condon mechanism of enhancement. Their UV−visible absorption spectra were also calculated spontaneously. On the basis of the RR spectra and computed results, the ground and excited-state structures as well as molecular packing of aggregated H_4TSPP^{2-} have been studied. It was deduced from the analyses that there are large dimensionless displacements on the excited state along the ν_8, γ_{16}, and ν_2 coordinates for both aggregated and segregated H_4TSPP^{2-}. These normal modes involve mainly the $C_\alpha C_m$, $C_\beta C_\beta$ bond stretching and $C_\alpha C_m C_\alpha$ bond angle bending motions. The low-frequency RR bands (<500 cm^{-1}) were greatly enhanced when the excitation wavelength approaches the J_B absorption band of H_4TSPP^{2-} aggregates, which was attributed to narrowing of the J_B band due to the exciton interaction. It was revealed that the 489 and 421 nm absorption bands of H_4TSPP^{2-} aggregates can be attributed to two different exciton manifolds originating from the degenerated B state (S_2 state) of H_4TSPP^{2-}. Davydov splitting of the aggregates evaluated from molecular exciton theory is well-coincident with the measured values, which supports a one-dimensional ribbon model for H_4TSPP^{2-} aggregates.

I. Introduction

The excited-state structure and properties of porphyrins are very important for understanding biologically important processes such as energy transfer in photosyntheses, photodynamic therapy of cancers, and chromophore−protein interaction in hemeproteins. Conventionally, the electronic excited-state properties of molecules or molecular assemblies can be extracted from high-resolution electronic absorption or emission spectroscopy and photoelectron spectroscopy. The bond-length and bond-angle changes of molecules on the excited states relative to the ground state can be evaluated from the intensities of corresponding electronic−vibrational transitions. Another method to obtain excited-state properties is resonance Raman (RR) intensity analysis, which is particularly useful for solution samples whose high-resolution electronic spectra and photoelectron spectra are usually difficult to obtain. Resonance Raman intensities have been well-formulated either in a traditional sum-over-states picture or equivalently in the time-dependent picture.[1−5] The Kramers−Kronig transform method has also been widely used to calculate RR excitation profiles from absorption spectrum of the scatter.[6,7] A considerable number of molecules have been studied with RR intensity analysis to investigate their excited-state structures and dynamics upon photoexcitation.[2,3,8−10]

Resonance Raman spectroscopy has been employed to study porphyrin and related compounds for many years.[11−17] These studies provide not only the knowledge of porphyrin molecules in the ground state but also the understanding of their electronic excited states. Spiro et al. has recently used the Kramers−Kronig transform method to analyze the RR intensities of nickel porphyrin (NiP).[18,19] In one of these works, the structural changes resulting from $S_0 \rightarrow S_2$ photoexcitation were computed using semiempirical quantum chemistry methods and projected onto the ground-state normal modes to calculate Raman intensities assuming validity of the Condon approximation for $S_0 \rightarrow S_2$ excitation. Their results indicate that the S_2 state (B state) of NiP is mainly due to a_{1a} (HOMO-1) $\rightarrow$ e_g*(LUMO) single-electron excitation, in coincident with other experimental and theoretical evidence.[18] In another paper, non-Condon contribution and interference effects were considered in $S_0 \rightarrow S_1$ excited Raman intensities of NiP.[19]

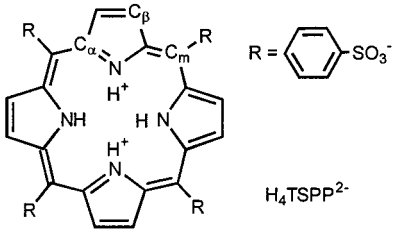

Figure 1. Structural sketch of tetrakis(4-sulfonatophenyl)porphyrin diacid (H_4TSPP^{2-}).

Porphyrin aggregates with regular high-order structures were attractive due to their structural resemblance to the chlorophyll aggregates. Therefore, spectroscopic studies of porphyrin aggregates may provide deeper understanding for molecular interaction and energy transfer in chlorophyll aggregates. Water soluble tetrakis(4-sulfonatophenyl)porphyrin (H_2TSPP^{4-}) is an important porphyrin derivative which has wide applications in many areas. Its *N*-diprotonated derivative (i.e., the diacid H_4TSPP^{2-}, whose structure is shown in Figure 1) was found to aggregate in highly acidic solution, accompanying dramatic changes in UV−visible absorption and luminescence spectra similar to J-aggregated

* Corresponding author. E-mail: fcliu@ustc.edu.cn

10.1021/jp003365e CCC: $20.00
Published on Web 04/03/2001

cyanine dyes.[20−23] The aggregation behavior of H_4TSPP^{2-} was found to sensitively depending on the concentration, ionic strength, and pH of solution.[20−22] The absorption spectrum of the aggregates was characterized by the appearance of a sharp band (denoted as J_B band) at 490 nm red-shifted by 56 nm compared with the B band (434 nm) of H_4TSPP^{2-} monomer. A broad and weak absorption at 421 nm (denoted as H_B band) was also observed in the aggregates. The origin of this blue-shifted absorption is not very clear, although it was suggested to be due to the formation of the H-aggregate (face-to-face structure) of H_4TSPP^{2-}.[22] Resonance Raman spectroscopy excited with 488.0 nm near the J_B absorption of aggregated H_4TSPP^{2-} (denoted as agg-H_4TSPP^{2-}) has been investigated by several authors, but no details about the excited state were elucidated.[24−26] Raman spectrum excited in resonance with the H_B band of agg-H_4TSPP^{2-} has not been reported yet to our knowledge. To bear these problems in mind, in the present paper, we have measured the Raman spectra of agg-H_4TSPP^{2-} with excitation light in resonance with both the J_B and H_B states. Spectra of molecular state H_4TSPP^{2-} (denoted as m-H_4TSPP^{2-}) were also studied for comparison. The Raman intensities of agg-H_4TSPP^{2-} were simulated by using time-dependent resonant Raman formulas (section IIIA). The ground-state structure of agg-H_4TSPP^{2-} was extracted from RR frequency changes due to the aggregation (section IIIB). The J_B and H_B excited-state structures of agg-H_4TSPP^{2-} were analyzed by using the theoretical simulation results, especially, the fitted parameters of the dimensionless displacement $|\Delta|$ and the line-width factor Γ (section IIIC, D). Finally, the molecular packing model and exciton splitting of agg-H_4TSPP^{2-} were elucidated on the basis of the exciton theory calculation (section IIIE).

II. Experimental and Theory

A. Experimental. Tetrasodium *meso*-tetrakis(4-sulfonatophenyl)porphyrin (TSPP·Na_4) was synthesized and purified according to the procedures described in the literature.[27,28] The aqueous solution of the free base H_2TSPP^{4-} (5×10^{-5} mol/L) was prepared by resolving TSPP·Na_4 in triply distilled water. Monomeric and aggregated diacid H_4TSPP^{2-} were prepared respectively by dropping a different amount of dilute H_2SO_4 (0.02 M) in H_2TSPP^{4-} aqueous solution. The final pH value was about 4 for m-H_4TSPP^{2-} and 1 for agg-H_4TSPP^{2-}. The prepared solutions were allowed to equilibrate for 5 h before measurements. For agg-H_4TSPP^{2-}, the samples were gently shaken prior to measurements. Raman spectra were recorded on a Spex-1403 double monochromator with 90° scattering geometry. The slit width of the monochromator was set such that the spectral resolution is 4 cm^{-1}. The 488.0, 496.5, and 457.9 nm lines of an Ar^+ laser and the 413.1 nm line of a Kr^+ laser were used as excitation sources with the power 60 mW.

B. Theory and Computational Method. In Albrecht and Tang's sum-over-states picture, Raman scattering is described in terms of the Kramers−Heisenberg−Dirac dispersion formula obtained by second-order perturbation theory.[1] Raman signals can be enhanced when the incident irradiation is resonant with an electronic transition, either due to the nonzero Franck−Condon overlap of the ground state and the resonant state (Albrecht's A-term mechanism) or due to the vibronic coupling betweent excited states (B-term mechanism). The A-term mechanism is dominant when incident radiation is in resonance with a strongly allowed electronic transition. In this situation the Raman scattering cross section of a molecule from initial vibrational state $|i\rangle$ to the final states $|f\rangle$ is given by[1−2,8]

$$\sigma_R(E_L,E_S) = \frac{8\pi e^4 E_S{}^3 E_L M^4}{9\hbar^4 c^4} \left|\sum_v \frac{\langle f|v\rangle\langle v|i\rangle}{(E_L - E_0 - \epsilon_v + \epsilon_i) - i\Gamma}\right|^2 \quad (1)$$

Here M is the electric dipole transition momentum, E_L and E_S are the energy of incident and scattering light, ϵ_i and ϵ_v are respectively the energy of the initial vibrational state $|i\rangle$ and the intermediate vibrational state $|v\rangle$, E_0 is the 0−0 electronic transition energy, Γ is the line-width factor. The summation in eq 1 covers all intermediate states that are transition dipole coupled to both initial and final states.

Formula 1 has been derived for nonaggregated molecules in homogeneous solution. The Raman polarizability of aggregated molecules has a similar form as segregated monomers assuming that the exciton−vibration interactions and vibrational coupling between the molecules are weak in the aggregate.[29,30] But exciton-coupling-induced changes on electronic energy levels and spectral line widths are necessarily considered for molecular aggregates with strong excited-state interactions.[31−34] As in the case of monomeric molecules, Raman scattering from aggregated molecules can be enhanced by the Franck−Condon mechanism when the excitation is in resonant with the molecular exciton absorption band (J band or H band) of the aggregates.[30] Thus, Raman cross section of a molecule in aggregate can still be described by eq 1, but E_0 and Γ are respectively the 0−0 transition energy and the line-width factor corresponding to the excitation from the ground state to a specific exciton state.

In this work, RR intensities and absorption spectra were calculated with the time-dependent method developed by Heller et al. and others.[4,5,8−10] Although it is theoretically equivalent with the sum-over-states method, the time-dependent method has been proven to be more efficient in computation for systems with many vibrational modes. The time-dependent expression of Raman scattering cross section corresponding to eq 1 is[8,9]

$$\sigma_R(E_L,E_S) = \frac{8\pi e^4 E_S{}^3 E_L M^4}{9\hbar^6 c^4} \left|\int_0^\infty \langle f|i(t)\rangle \exp[i(E_L - E_0 + \epsilon_i)t/\hbar]\exp[-\Gamma t/\hbar]dt\right|^2 \quad (2)$$

The light absorption cross section is given as

$$\sigma_A(E_L) = \frac{4\pi e^2 E_L M^2}{3\hbar^2 cn} \mathrm{Re}\left[\int_0^\infty \langle i|i(t)\rangle \exp[i(E_L - E_0 + \epsilon_i)t/\hbar]\exp[-\Gamma t/\hbar]dt\right] \quad (3)$$

where n is the solvent index of refraction. The time-dependent function $|i(t)\rangle = \exp(-i\mathbf{H}t/\hbar)|i\rangle$ stands for the time evolution of vibrational wave function $|i\rangle$ on the excited-state potential surface, where $\mathbf{H}$ is the vibrational Harmitonian on the excited state. Formula 2 manifests that the intensity of a Raman band depends on the overlapping calculus $\langle f|i(t)\rangle$ of motional wave packet $|i(t)\rangle$ with the final vibration state $|f\rangle$. To simplify the overlap, the following approximations are employed: (1) both the ground- and excited-state potential surfaces are assumed to be harmonic; (2) there is no Duschinsky rotation; i.e. the normal mode compositions at excited state are the same as those at ground state; and (3) the force constants of excited and ground states are the same; i.e., the potential surface of the excited state is shifted but not distorted compared with that of ground state.

With these approximations, the overlap $\langle f|i(t)\rangle$ can then be written as the following simple form[8]

TABLE 1: Parameters for Simulations of Resonance Raman Spectra and UV−Visible Spectra of agg-H_4TSPP^{2-} and m-H_4TSPP^{2-}

agg-H_4TSPP^{2-} [a]		agg-H_4TSPP^{2-} [b]		m-H_4TSPP^{2-} [c]			
ν/cm^{-1}	$\|\Delta\|$(J_B state)	ν/cm^{-1}	$\|\Delta\|$ (H_B state)	ν/cm^{-1}	$\|\Delta\|$ (B state)	ν_i [d]	assign. [e]
1594	0.065	1594	0.065	1599	0.065		phenyl ν(C═C)
1563	0.064	1563	0.049	1569	0.048	ν_{10}	$\nu(C_\alpha C_m)$
1538	0.149	1538	0.124	1546	0.116	ν_2	$\nu(C_\beta C_\beta)/\nu(C_\alpha C_m)$
		1493	0.059				
1477	0.084	1474	0.059	1479	0.065	ν_3	$\nu(C_\alpha C_m)/\nu(C_\beta C_\beta)$
1430	0.056						
1384	0.036	1371	0.110	1371	0.076	ν_4	$\nu(C_\alpha C_\beta)/\nu(C_\alpha N)$
1356	0.032	1356	0.087	1342	0.038	ν_{12}	$\nu(C_\alpha N)/\nu(C_\alpha C_\beta)$
1321	0.067			1327	0.038		
1283	0.034						
1232	0.116	1232	0.150	1239	0.145	ν_1	$\nu(C_m Ph)$
				1202	0.052		
1123	0.043	1122	0.049	1128	0.060	ν_9	$\delta(C_\beta H)$
1083	0.062	1081	0.037	1088	0.069	ν_{17}	$\delta(C_\beta H)$
1017	0.101	1016	0.064	1011	0.091	ν_{15}	$\nu(C_\alpha C_\beta)/\nu(C_\alpha N)$
987	0.133	987	0.091	972	0.075	ν_6	$\nu(C_\alpha C_\beta)/\nu(C_\alpha N)$
914	0.046	918	0.058				
880	0.037						
807	0.032			809	0.062		
		730	0.046				
700	0.109	700	0.05	704	0.094	ν_7	$\delta(NC_\alpha C_m)/\nu(C_\alpha N)$
		670	0.057				
		622	0.053				
582	0.078						
		419	0.104	435	0.108		
364	0.090			409	0.115		
317	0.310	317	0.201	315	0.271	ν_8	$\delta(C_\alpha C_m C_\alpha)/\nu(C_\alpha C_m)$
242	0.365	238	0.194	235	0.312	γ_{16}	$\delta(C_\alpha C_m C_\alpha)/\nu(C_\alpha C_m)$

[a] $E_0 = 20380$ cm^{-1}, $M = 3.35$ Å, $n = 1.333$, $\Gamma = 142$ cm^{-1}. [b] $E_0 = 23656$ cm^{-1}, $M = 2.09$ Å, $n = 1.333$, $\Gamma = 457$ cm^{-1}. [c] $E_0 = 22998$ cm^{-1}, $M = 3.75$ Å, $n = 1.333$, $\Gamma = 410$ cm^{-1}. [d] Mode order from refs 13 and 14. [e] From refs 13, 14, and 26.

$$\langle f|i(t)\rangle = \left\{\exp\left[-\frac{\Delta^2}{2}(1 - e^{-i\epsilon t/\hbar})\right] [\exp(-i\epsilon t/\hbar) - 1]^f \frac{\Delta^f}{(2^f f!)^{1/2}}\right\} \quad (4)$$

Here, Δ is the dimensionless displacement of excited-state equilibrium nuclear geometry relative to the ground state along a specific normal coordinate, and ϵ and f are respectively the energy and quantum number of the corresponding normal coordinate.

In this paper, simulation of RR and UV−visible absorption spectra of agg-H_4TSPP^{2-} and m-H_4TSPP^{2-} were performed with time-dependent-method with formulas 2−4 for a temperature of 300 K.[35] Calculation parameters were iteratically adjusted to fit the measured RR intensities and absorption spectra in the 380−520 nm region (B band region for porphyrin compounds). Simulation for absorption and RR spectra was carried out with the same set of parameters for each excited-state involved. The simulation results are shown in Table 1

III. Results and Discussion

A. Experimental and Computational Results. The UV−visible absorption bands of porphyrins are due to the electronic transitions from the ground state (S_0) to the two lowest singlet excited states S_1 (Q state) and S_2 (B state). The $S_0 \rightarrow S_1$ transition gives rise to the weak Q bands in the visible region (550−650 nm), while the $S_0 \rightarrow S_2$ transition produces a strong B band in the near-UV region (400−450 nm). For m-H_4TSPP^{2-}, these transitions were observed at 434 nm (B band) and 632 nm (Q_{00} band). In agg-H_4TSPP^{2-}, these bands shift to 421 nm (H_B band), 490 nm (J_B band), and 706 nm (J_Q band) respectively, which was attributed to the exciton coupling.[20−23] Figure 2 displays the experimental and calculated absorption spectra of molecular exciton bands (H_B at 421 nm and J_B at 490 nm) of agg-H_4TSPP^{2-} and the B absorption band (434 nm) of m-H_4TSPP^{2-}. The positions of incident radiation for RR measurements are marked as arrows in Figure 2. In our RR measurements, the wavelength positions of incident light are well close to the J_B and H_B transitions of agg-H_4TSPP^{2-} or the B band transition of m-H_4TSPP^{2-}. The interference of the Q state (S_1 state) of H_4TSPP^{2-} to the RR intensities is insignificant, owing to the

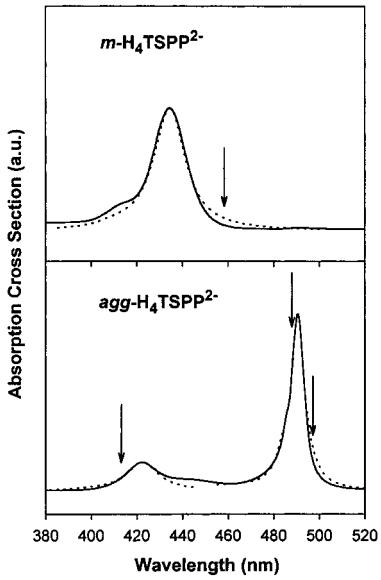

Figure 2. Experimental (solid line) and calculated (dash line) absorption spectra for agg-H_4TSPP^{2-} and m-H_4TSPP^2. The arrows mark the positions of the excitation wavelength in Raman experiments.

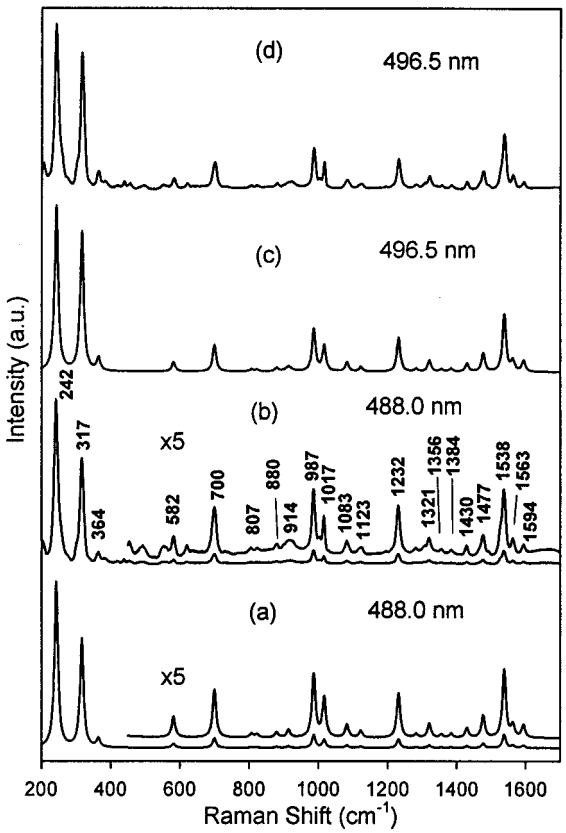

Figure 3. Calculated (a, c) and experimental (b, d) Raman spectra of agg-H_4TSPP^{2-} excited at 488.0 and 496.5 nm. Laser power, 60 mW; time constant = 1 s/cm^{-1}; concentration of H_4TSPP^{2-}, ~ 0.1 mM; pH ~ 1.

weak strength of the $S_0 \rightarrow S_1$ transition and the large energy difference between the excitation light and the $S_0 \rightarrow S_1$ transition.

Figure 3 compares the experimental and calculated Raman spectra of agg-H_4TSPP^{2-} excited at 488.0 and 496.5 nm, which are in resonance or near-resonance with the J_B state. It is noticeable that the intensities of the Raman bands in the low-frequency region (<500 cm^{-1}) relative to those in high-frequency region change dramatically from the 488.0 nm excited spectrum to the 496.5 nm excited one. For instance, the 242 and 317 cm^{-1} bands are almost 10 times stronger than the high-frequency band at 1538 cm^{-1} with 488.0 nm excitation, whereas this ratio changes to about 3 times with 496.5 nm excitation. Figure 4 displays the measured Raman spectra of agg-H_4TSPP^{2-} and its deuterated derivative agg-D_4TSPP^{2-} excited at 413.1 nm (near H_B absorption) as well as the calculated spectrum of agg-H_4TSPP^{2-}. The experimental and calculated RR spectra of m-H_4TSPP^{2-} excited at 457.9 nm are displayed in Figure 5. While the low-frequency bands at 235 and 315 cm^{-1} in Figure 5 are still among the strongest bands, their intensities are not as predominant as their counterparts in agg-H_4TSPP^{2-} (the 242 and 317 cm^{-1} bands of Figures 3). Table 1 lists the parameters for the best fitting of the measured UV−visible spectra and RR intensities. It should be noticed that both the 0−0 transition position (E_0) and spectral width (Γ) of agg-H_4TSPP^{2-} are different from those of m-H_4TSPP^{2-}.

B. RR Frequencies and Ground-State Structure of agg-H_4TSPP^{2-}. The differences of vibrational frequencies between the agg-H_4TSPP^{2-} and m-H_4TSPP^{2-} reflect their structural differences in ground state. For porphyrin-related compounds, the RR bands in the 1450−1650 cm^{-1} region involve the stretch of the $C_\beta-C_\beta$ and $C_\alpha-C_m$ bonds due to the relatively large force constants of these bonds. The RR bands

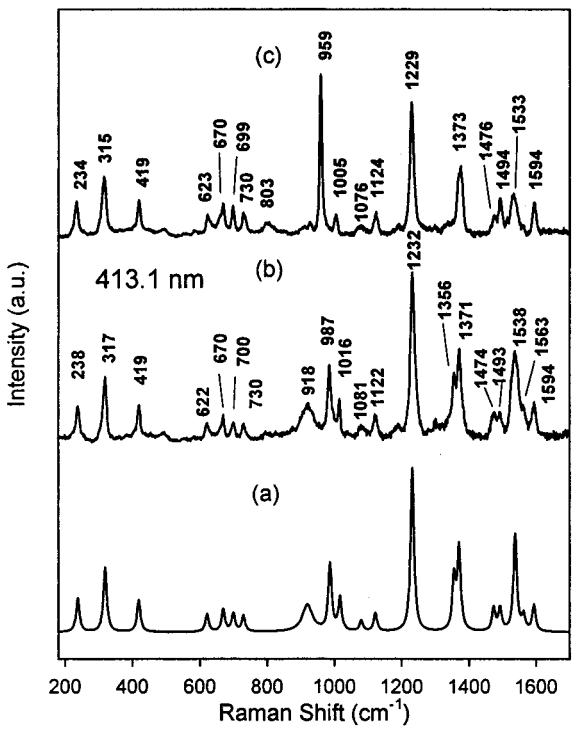

Figure 4. Calculated (a) and experimental (b) Raman spectra of agg-H_4TSPP^{2-} excited at 413.1 nm; (c) experimental Raman spectra of agg-D_4TSPP^{2-} excited at 413.1 nm. Laser power, 60 mW; time constant = 1 s/cm^{-1}; concentration of H_4TSPP^{2-} (D_4TSPP^{2-}), ~0.1 mM; pH (pD) ~ 1.

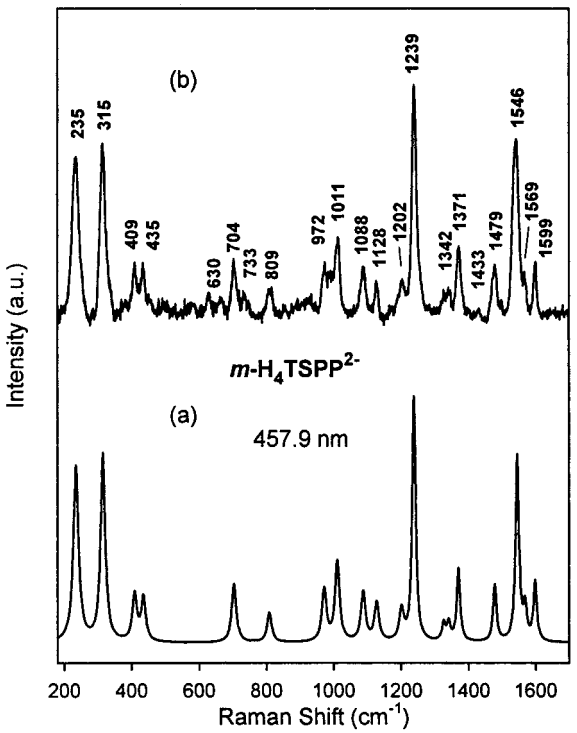

Figure 5. Calculated (a) and experimental (b) Raman spectra of m-H_4TSPP^{2-} excited at 457.9 nm. Laser power, 60 mW; time constant = 1 s/cm^{-1}; concentration of H_4TSPP^{2-}, ~ 0.1 mM; pH ~ 4.

in the 1300−1450 cm^{-1} region are due to the $C_\alpha-C_\beta$ and $C_\alpha-N$ stretching motions, which are thought to mix with each other severely.[13,14] Compared with m-H_4TSPP^{2-}, the $C_\alpha-C_m$ and $C_\beta-C_\beta$ stretching frequencies (1538 cm^{-1} for ν_2 and 1563 cm^{-1} for ν_{10}) of agg-H_4TSPP^{2-} decrease by 6−8 cm^{-1}cm^{-1}, while $C_\alpha-C_\beta/C_\alpha-N$ stretching frequencies (ν_4, ν_{15}, and ν_{12}) increase

by 6−13 cm^{-1}, indicating that agg-H_4TSPP^{2-} has prolonged $C_\alpha-C_m$ and $C_\beta-C_\beta$ bonds and shortened $C_\alpha-C_\beta$ and $C_\alpha-N$ bonds compared with m-H_4TSPP^{2-}. The porphyrin skeleton of the diacids are known to be saddled, owing to the stereo hindrance of four hydrogen atoms in the center.[36] The observed structural changes from m-H_4TSPP^{2-} to agg-H_4TSPP^{2-} probably reflect the general trends when a saddle-shaped porphyrin become more planar. There are reports in the literature which broadly show these trends.[37] For instance, the frequencies for the ν_2 mode of the metal complexes of octaethyltetraphenylporphyrin (OETPP), a very saddled porphyrin, shift to lower frequency by 30−40 cm^{-1} compared with the corresponding mode of the planar metallooctaethylporphyrins (MOEPs).[37]

The 242 cm^{-1} band of agg-H_4TSPP^{2-} (Figure 3) and the 235 cm^{-1} band of m-H_4TSPP^{2-} (Figure 5) are tentatively assigned to the out-of-plane saddling mode γ_{16} (B_{2u} symmetry under D_{4h}) of the porphyrin ring, which is probably coupled with the in-plane motion.[14] The 317 cm^{-1} band of agg-H_4TSPP^{2-} and the 315 cm^{-1} band of m-H_4TSPP^{2-} were attributed to the in-plane breathing mode of the porphyrin-ring (ν_8).[13,26] For most of the planar porphyrin compounds, such as H_2TSPP^{4-} (D_{2h}) and NiP (D_{4h}), the ν_8 mode, but not the γ_{16} mode, is strongly enhanced with near-B band excitation, since the B band is in-plane $\pi\rightarrow\pi^*$ transition in character. In porphyrin diacid H_4TSPP^{2-}, however, the effective symmetry of the porphyrin ring reduces to D_{2d}.[36] Since the γ_{16} and ν_8 modes have the same A_1 symmetry under D_{2d}, they are expected to strongly mix with each other, and both are resonantly enhanced via the Franck−Condon mechanism.[11,12] The out-of-plane mode at 235 cm^{-1} (γ_{16}) in m-H_4TSPP^{2-} shifts to 242 cm^{-1} in agg-H_4TSPP^{2-}, reflecting that the molecular packing in aggregate induces a constraint for the out-of-plane motion of the porphyrin ring. This is also consistent with the prolonged $C_{\alpha-}C_m$ and $C_{\beta-}C_\beta$ bonds and shortened $C_{\alpha-}C_\beta$ and $C_{\alpha-}N$ bonds of agg-H_4TSPP^{2-} compared with those of m-H_4TSPP^{2-}, which can be rationalized by assuming that the H_4TSPP^{2-} molecules in the aggregates adapt a more planar conformation to optimize the $\pi-\pi$ interaction with each other.

Most RR frequencies of agg-H_4TSPP^{2-} with 413.1 nm excitation are coincident with the 488.0 or 496.5 nm excited ones, implying that "the 421 nm species" is identical with "the 489 nm species". An obvious exception is the strong 238 cm^{-1} band in the 413.1 nm spectrum, which is downward shifted by 4 cm^{-1} compared with the 242 cm^{-1} band in the 488.0 and 496.5 nm excited spectra. In D_2O solution, the 238 cm^{-1} band of agg-H_4TSPP^{2-} (413.1 nm excitation) shifts to 234 cm^{-1} due to the deuteration of central hydrogen atoms (Figure 4). Similarly, by using 488.0 nm excitation, the 242 cm^{-1} band of agg-H_4TSPP^{2-} shifts to 238 cm^{-1} in D_2O solution (which has been recorded but not shown here). The identical deuteration shifts and dominant intensities hint at a close connection between the 242 cm^{-1} band with J_B resonant excitation and the 238 cm^{-1} with H_B resonant excitation. We suggest that these two bands come from the same vibration of the H_4TSPP^{2-} molecule, which is split by molecular interaction and selectively enhanced respectively with H_B and J_B resonant excitation.

On the whole, the differences of vibrational frequencies in the RR spectra of agg-H_4TSPP^{2-} and m-H_4TSPP^{2-} indicate the ground-state structure changes due to the aggregation. To go a step further, the intensity analysis of the RR spectra of agg-H_4TSPP^{2-} using the time-dependent resonance Raman theory can extract the structural information of agg-H_4TSPP^{2-} in J_B and H_B excited states that are presented in the following sections.

C. Structure of agg-H_4TSPP^{2-} on J_B and H_B Excited States. The simulations of RR spectra and UV−visible absorption spectra of agg-H_4TSPP^{2-} and m-H_4TSPP^{2-} are performed with the time-dependent method and the calculation results are shown in Table 1. Among the fitted parameters, the dimensionless displacement $|\Delta|$ and the line-width factor Γ are essential to the intensity analysis. The dimensionless displacement $|\Delta|$ reflects excited-state geometry changes relative to the ground-state projecting along the corresponding normal coordinate. Transforming dimensionless displacements into absolute changes of bond length and bond angle requires the compositions of normal coordinates, which are not available for H_4TSPP^{2-} at present. However, the assignments of the Raman bands of agg-H_4TSPP^{2-} have been proposed,[24,26] providing valuable references for discussion of its exciton state structural features. For the J_B state, the 242 cm^{-1} (γ_{16}) and 317 cm^{-1} (ν_8) bands have the largest dimensionless displacements, 0.365 and 0.310, respectively (Table 1). The γ_{16} and ν_8 modes involve mainly the $C_\alpha C_m C_\alpha$ bending and $C_\alpha C_m$ stretching motions.[14,26] Therefore, the large $|\Delta|$ values of γ_{16} and ν_8 modes indicate large changes for $C_\alpha C_m C_\alpha$ bond angle and $C_\alpha C_m$ bond length on the J_B state compared with the ground state. In the high-frequency region (>900 cm^{-1}), the 1538 cm^{-1} band (ν_2), which involves $C_\beta C_\beta$ and $C_\alpha C_m$ bond stretches, has large dimensionless displacement ($|\Delta| = 0.149$). Other modes with large $|\Delta|$ values at J_B state are the 1232 cm^{-1} (ν_1, C_m-Ph stretch, $|\Delta| = 0.116$) and 987 cm^{-1} band (ν_6, $C_\alpha C_\beta$ and $C_\alpha N$ bond stretches, $|\Delta| = 0.133$). Compared with ν_8 and γ_{16}, the $|\Delta|$ values of ν_1, ν_2, and ν_6 are much smaller. Since absolute displacements are proportional with the dimensionless displacements while inversely proportional with the square-root of normal frequencies,[8] low-frequency modes such as ν_8 and γ_{16} are expected to have much larger absolute displacements. Thus, the bond-length changes on the J_B state are deduced in the order $C_\alpha C_m > C_\beta C_\beta > C_m-Ph > C_\alpha C_\beta \sim C_\alpha N$. Besides, large changes for $C_\alpha C_m C_\alpha$ bond angles are expectable.

It is known that the RR spectra of the porphyrins usually show distinctive and characteristic enhancement patterns when excitation light is in resonance with different electronic transitions. For agg-H_4TSPP^{2-}, the intensity pattern of the 413.1 nm excited spectrum in 900−1700 cm^{-1} is similar to the 488.0 and 496.5 nm excited ones. For instance, the RR bands such as 987, 1016, 1232, 1538, and 1594 cm^{-1} were measured with comparable relative intensities in Figures 3 and 4. Simulation of RR and absorption spectra reveals large dimensional displacements for the ν_1 ($|\Delta| = 0.150$), ν_2 ($|\Delta| = 0.124$), ν_8 ($|\Delta| = 0.201$), and γ_{16} ($|\Delta| = 0.194$) modes on the H_B state, similar to the cases of the J_B state. It is noted that these vibrational modes also correspond to large dimensionless displacements for m-H_4TSPP^2 on the B state. This evidence hints that both the H_B and J_B states of agg-H_4TSPP^{2-} have an origination connecting with the B state of the H_4TSPP^{2-}molecule. As shown in section IIIE, the H_B and J_B states of agg-H_4TSPP^{2-} can be attributed to two exctonic manifolds from the degenerated B state of H_4TSPP^{2-} which is split by molecular interaction.

The relative intensities of low-frequency bands compared with the high-frequency bands for the H_B state resonant spectra in Figure 4 are not as large as with J_B state resonant spectra (Figure 3). In the 600−750 cm^{-1} region, four middle strong RR bands were observed at 622, 670, 700, and 730 cm^{-1} with 413.1 nm excitation, in contrast to the 488.0 or 496.5 nm excited spectra in which the intensity of the 700 cm^{-1} band is obviously prevailing. The strong band at 419 cm^{-1} in the 413.1 nm excited spectrum was not observed with 488.0 and 496.5 nm excitations. This band is tentatively assigned to a deformational mode of the porphyrin macrocycle according to its frequency position

and rather strong intensity. The distinctions in intensity patterns between the RR spectra with J_B and H_B resonant excitation may be attributed to the different directions of polarization for J_B and H_B transitions (section IIIE), which are expected to selectively enhance different vibrations.

The $|\Delta|$ values of m-H_4TSPP^{2-} are very close to those of agg-H_4TSPP^{2-} for most RR bands. As shown in Table 1, both species have relatively large $|\Delta|$ values for ν_8, γ_{16}, ν_2, ν_1, and ν_6 modes but small $|\Delta|$ values for ν_{10}, ν_3, ν_{12}, and ν_{17} modes. This similarity manifests that the structural changes of agg-H_4TSPP^{2-} from the ground state to the exciton state (J_B or H_B states) are similar to those of m-H_4TSPP^{2-} resulting from the corresponding electronic transition (S_0 to S_2). This reflects the fact that the molecular excitons in aggregates are Frenkel excitons.[32,33] Despite that the excited electronic state extends over many molecules in aggregate, the intramolecular properties of the excited state persist.

D. Influence of Line-Width Factor Γ On RR Intensities. The presence of enhanced low-frequency bands for aggregated molecules is an interesting phenomenon.[38,39] With the intensity of the high-frequency band ν_2 (1563 cm^{-1}) as an internal standard, the relative intensity of ν_8 (or γ_{16}) with 488.0 nm excitation is about 3 times larger than that with 496.5 nm excitation. This striking change in relative intensities upon excitation wavelength can be attributed to the inherent narrowness of the exciton transition, as evidenced by the sharp J_B absorption band in the UV−visible spectrum of agg-H_4TSPP^{2-}. For very small excited-state displacements, the factor $\exp[-(\Delta^2/2)(1 - e^{-i\epsilon t/\hbar})]$ in eq 4 can be replaced approximately by unity. The Raman intensity of the kth fundamental can thus be expressed as

$$I_k = K\Delta_k^2 \left|\int_0^\infty [\exp(-i\epsilon_k t/\hbar) - 1] \exp[i(E_L - E_0)t/\hbar]\exp[-\Gamma t/\hbar]dt\right|^2$$

$$= K\hbar^2\epsilon_k^2\Delta_k^2 \frac{1}{[(E_0 - E_L)^2 + \Gamma^2][(E_0 - E_L + \epsilon_k)^2 + \Gamma^2]} \quad (5)$$

where K is a constant containing the transition dipole moment and the concentration of the scatter. Blazej and Peticolas have derived the same formula from the sum-over-states approach several years ago.[40] Formula 5 hints that, in addition to the Δ values connected with Franck−Condon factors, RR intensities also sensitively depend on the line-width factor Γ of the electronic (or exciton) transition in the resonant. The relative intensity of ν_8 versus ν_2 for 488.0 and 496.5 nm excitations can be given by

$$\frac{(I_{\nu_8}/I_{\nu_2})_{488}}{(I_{\nu_8}/I_{\nu_2})_{496}} = \frac{[(E_0 - E_{496} + \epsilon_{\nu_8})^2 + \Gamma^2]/[(E_0 - E_{496} + \epsilon_{\nu_2})^2 + \Gamma^2]}{[(E_0 - E_{488} + \epsilon_{\nu_8})^2 + \Gamma^2]/[(E_0 - E_{488} + \epsilon_{\nu_2})^2 + \Gamma^2]}$$

With Γ as 142 cm^{-1} for the J_B band, the calculated $(I_{\nu_8}/I_{\nu_2})_{488}/(I_{\nu_8}/I_{\nu_2})_{496}$ ratio is about 3.38, consistent with the experimental value of 3.33. Similar dramatic enhancement in relative intensity for low-frequency bands has also been found in aggregated cyanine dyes upon resonance excitations with J absorption bands.[38,39] Akins et al. have developed an aggregation-enhanced Raman scattering (AERS) theory and explained successfully this enhancement for aggregated cyanine dyes.[29] According to the AERS mechanism, the term in the denominator of the Raman intensity expression become small as the resonance is approached, leading to enhanced Raman scattering.[29] Implicit in this picture is the dependence of Raman intensity on line-width change. Thus, the unusual enhancement of low-frequency bands upon resonance excitation of J bands can be thought to connect with the dramatic narrowing of spectral line width caused by exciton coupling. We noted that, due to the broad H_B absorption and large line-width factor $\Gamma = 457$ cm^{-1}, the intensities of the low-frequency RR bands of agg-H_4TSPP^{2-} with H_B resonant excitation (Figure 4) are not as dominant as their counterparts in the J_B excited spectra (Figure 3).

The foregoing results in sections IIIB−D indicate that the RR spectra and their theoretical simulation for the agg--H_4TSPP^{2-} molecule are a useful probe of the ground- and excited-state structures of a molecule in the aggregated system. However, for the elucidation of the regular high-order structures and aggregation nature of agg-H_4TSPP^{2-}, the theoretical analysis of UV−visible absorption spectra is vital and will be presented in the next section.

E. Excitonic Splitting and Molecular Packing In agg-H_4TSPP^{2-}. The nature of the violet band at 421 nm of agg-H_4TSPP^{2-} has not been well-understood yet. This band has been found polarized perpendicular to the long axis of the aggregate.[23] Ribo et al. suggested that it is due to a new face-to-face aggregate (H-aggregate) of H_4TSPP^{2-}.[22] However, H-aggregation seems not favorable in the view of the electrostatic repulsion between adjacent H_4TSPP^{2-} molecules. We have used the exciton theory to calculate the blue shift of the B band with the H-aggregation model (face-to-face packing). It turns out that the calculated blue shift with the H-aggregation model is at least 10 times larger than the experimental value (711 cm^{-1}). Thus, it seems more plausible to attribute the J_B and H_B bands to different exciton manifolds; both originated from the B band of H_4TSPP^{2-}. Splitting of the B band of aggregated H_4TSPP^{2-} can be considered as the reasonable consequence of the symmetry lowering of the porphyrin macrocycle in aggregates. Moreover, the degeneracy in the B state can be lifted by exciton interactions for which the angle between the line-of-centers and the x-component of the in-plane dipole (M_x) is different from that between the line-of-centers and the y-component of the in-plane dipole (M_y). The lift of the degeneracy of the B state due to the exciton interactions has also been observed in aggregated protoporphyrin IX glycosamides [41] and porphyrin monolayer assemblies.[42]

Molecular packing of agg-H_4TSPP^{2-} has been proposed as a one-dimensional linear chain on the basis of the electrostatic interaction model.[22,24] Since H_4TSPP^{2-} is a zwitterionic molecule, the positively charged center of one H_4TSPP^{2-} molecule can attract the negatively charged peripheral substituents of the adjacent molecules; thus, the linear assembly of H_4TSPP^{2-} molecules can be constructed. Excess cations (H^+, Na^+, or K^+, for instance) are required to shield the electrostatic repulsion of the anionic sulfonate groups of adjacent molecules. Figure 6 plots the structural model of agg-H_4TSPP^{2-}, where the geometric parameters were evaluated from the crystallographic data of tetraphenylporphyrin diacid (H_4TPP^{2+}).[36] With this structural model, exciton theory is now employed to calculate the energy shift of the J_B and H_B states of agg-H_4TSPP^{2-} relative to the B state of m-H_4TSPP^{2-}. For simplicity, we neglect the nonplanarity of the porphyrin core and the possible twist or rumple of the aggregates. We believe that neglecting the nonplanarity of the porphyrin macrocycle does not introduce significant error, since the intermolecular distance, which is the key factor for

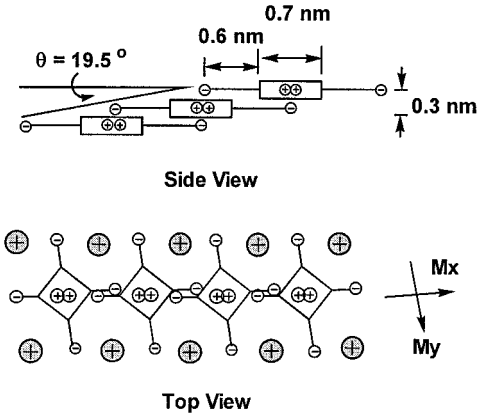

Figure 6. Structure model of H_4TSPP^{2-} aggregate. The shadowed cycles represent the external cations.

the calculation of the spectral split, does not change much. Similar simplified models have been successfully used to calculate the exciton split of aggregated protoporphyrin IX glycosamides.[41] The coordinate system in Figure 6 is chosen so that the porphyrin plane is the *XY*-plane and the *Y*-axis is perpendicular to the line through the molecular centers. According to the strong coupling model of the molecular exciton, the energy of the single-exciton transition for an infinite linear chain is given by: $\Delta E = \Delta E_0 + 2V$, where interaction potential V can be calculated with point dipole model.[31] The sign of V, which depends on the molecular arrangement in the aggregates, determines whether the exciton band is red-shifted or blue-shifted relative to the corresponding monomer absorption.

With the approximation of nearest neighbor interaction, the interaction potential with point dipole model is described as

$$V_x = \frac{M_x^2}{r^3}(1 - 3\cos^2\theta) \quad \text{and} \quad V_y = \frac{M_y^2}{r^3}$$

where $r = 10.0$ Å is the distance of the transition dipole moments and $\theta = 19.5°$ is the angle between the line-of-centers and the in-plane dipole M_x. The fact that the in-plane dipole M_y is perpendicular to the line-of-centers has been taken in account in the expression of V_y. The magnitude of M can be estimated from the integrated intensity of the corresponding absorption bands. The integrated absorption coefficient of the B band of m-H_4TSPP^{2-} (1.29×10^{19} $mmol^{-1}\cdot cm^2\cdot s^{-1}$) gives the transition electric dipole strength $M^2 = 166$ D^2 as the sum of two components (M_x^2 and M_y^2) of the degenerate B transition.[22] The ratio of the square of the transition dipole M_x^2/M_y^2 was estimated from the UV−visible absorption spectra by

$$\frac{M_x^2}{M_y^2} = \frac{A_J/\lambda_J}{A_H/\lambda_H}$$

where the absorption ratio A_J/A_H can be estimated from the measured relative peak intensities (6.6:1 for J_B vs H_B) and fwhh (1:3.5 for J_B vs H_B). It follows that the transition strength M_x^2 and M_y^2 equal 114 D^2 and 52 D^2, respectively. The Davydov splitting was calculated respectively as -1993 cm^{-1} (for the red-shifted band) and 526 cm^{-1} (for the blue-shifted band), significantly deviated from the measured values of -2640 and 711 cm^{-1}. This manifests that the contributions from residue molecules other than the nearest neighbors are important. When interaction of all molecules in the aggregate is considered, the spectral shift of the exciton band of the aggregates relative to the corresponding electronic transition of monomer is amplified by a factor of 1.202 compared with the value from the nearest neighbor approximation.[43] Therefore, the calculated spectral shifts are -2395 cm^{-1} (J_B) and 632 cm^{-1} (H_B), respectively, with long-range interaction. In view of the approximations (point−dipole interaction and flat instead of twisted or folded ribbon), the coincidence between calculated and measured spectral shifts is fairly satisfying. It thus further supports the idea that the 421 and 489 nm absorption bands of agg-H_4TSPP^{2-} are due to different exciton manifolds with B band origination.

Before closing this report, it is necessary to discuss the theoretical approximations used in eq 4. Due to the lack of detailed information about the excited-state potential surfaces for H_4TSPP^{2-}, a set of the so-called "standard assumptions"[1] are introduced in eq 4 as the first step for the practical computation. Similar approximations have been used to simulate the B band excited RR intensity of nickel porphyrin (NiP) and were proven successful.[18] Deviations from the "standard assumptions" include non-Condon effects, quadratic vibronic coupling effects [the force constant changes and mode mixing (Duschinsky rotation)], anharmonic corrections appearing at higher order, and nonadiabatic effects at one of the most refined levels.[1] Hassing and Mortensen have provided perhaps the most comprehensive treatment for the Duschinsky effects.[44] They have shown that the Duschinsky terms and the nonadiabatic terms are of the same order of magnitude. However, extensive Duschinsky rotation does occur in porphyrin. Zgierski et al. have applied Duschinsky mixing effect along with the vibronic interference modes to account for the Raman excitation profiles of copper tetraphenylporphyrin.[17] Thus further works for aggregated H_4TSPP^{2-} are necessary to include all possible contributions from vibronic coupling, Duschinsky effect, and other approximations.[1] This is difficult for practical calculation at the present time. If Duschinsky rotation and/or anharmonicities are considered, the time-domain method loses some of its advantages in the view of calculation efficiency. Nevertheless, explicit forms for $\langle f|i(t)\rangle$ have been given in the literature for the cases of unequal ground- and excited-state vibrational frequencies as well as Duschinsky rotation.[8] There are also other theoretic approaches to treat the multimode problem of resonant Raman scattering.[1] Using a different approach, Shelnutt et al. have considered a variety of problems involved in the calculation of Raman excitation profiles, including nonadiabatic, interference, and Duschinsky effects.[15]

IV. Concluding Remarks

In summery, we have analyzed the RR intensities of aggregated and nonaggregated H_4TSPP^{2-}. Mode-specific structural changes on the excited state relative to the ground state are discussed. There are large dimensionless displacements along ν_8, γ_{16}, ν_2, ν_6, and ν_1 normal modes in the excited state, with the ν_8 and γ_{16} modes having the maximum $|\Delta|$ values, for both of agg-H_4TSPP^{2-} and m-H_4TSPP^{2-}. On the basis of the internal coordinate compositions of normal modes, we conclude that the bond-length differences between excited and ground states follow the order $C_\alpha C_m > C_\beta C_\beta > C_m - Ph > C_\alpha C_\beta \sim C_\alpha N$, accompanying large alteration for $C_\alpha C_m C_\alpha$ bond angles. The 489 and 421 nm absorption bands were attributed to two exciton manifolds originating from the degenerated B state (S_2 state) of H_4TSPP^{2-}. One-dimensional chain model of H_4TSPP^{2-} aggregate was supported by the Davydov splitting of the aggregates evaluated from molecular exciton theory. The present work demonstrates that RR intensity analyses can be used to extract properties of aggregates on exciton states, which may be very valuable for understanding important processes such

as spectral sensitization in photographic science and energy transfer in photosynthetic systems.

Acknowledgment. D.M.C. is grateful to Prof. A. B. Myers for providing programs for Raman intensity calculations. This work was supported by the National Natural Science Foundation of China (Grant No.: 29873043) and the Research Fund for the Doctoral Program of Higher Education (RFDP).

References and Notes

(1) (a) Tang, J.; Albrecht, A. C. In *Raman Spectroscopy*; Szymanski, H. A., Ed.; Plenum Press: New York, 1970; Vol. 2, p 33. (b) Champion, P. M.; Albrecht, A. C. *Annu. Rev. Phys. Chem.* **1982**, *33*, 353.

(2) Clark, R. J. H.; Dines, T. J. *Angew. Chem., Int. Ed. Engl*. **1986**, *25*, 131.

(3) Zink, J. I.; K., K.-S. *Adv. Photochem.* **1991**, *16*, 119.

(4) Lee, S.-Y.; Heller, E. J. *J. Chem. Phys*. **1979**, *71*, 4777.

(5) Heller, E. J.; Sundberg, R. L.; Tannor, D. *J. Phys. Chem.* **1982**, *86*, 1822.

(6) Tonks, D. L.; Page, J. B. *Chem. Phys. Lett*. **1979**, *66*, 449.

(7) Blazej, D. C.; Peticolas, W. L. *J. Chem. Phys.* **1980**, *72*, 3134.

(8) (a) Myers, A. B. In *Laser Techniques in Chemistry;* Myers, A. B,. Rizzo, T. R., Eds.; Wiley-Interscience: New York, 1995; Vol 23, p 325. (b) Myers, A. B. *J. Raman Spectrosc.* **1997**, *28*, 389.

(9) Lawless, M. K.; Wickham, S. D.; Mathies, R. A. *Acc. Chem. Res.* **1995**, *28*, 493.

(10) Kelley, A. M. *J. Phys. Chem. A*, **1999**, *103*, 6891.

(11) Spiro, T. G.; Li, X.-Y. In *Biological Application of Raman Spectroscopy*; Spiro, T. G., Ed.; Wiley-Interscience: New York, 1988; Vol. 3, p 1.

(12) Kitagawa, T.; Ozaki, Y. *Struct. Bonding*, **1987**, *64*, 71.

(13) Li, X.-Y.; Czernuszewicz, R. S.; Kincaid, J. R.; Su, Y. O.; Spiro, T. G. *J. Phys. Chem.* **1990**, *94*, 4**,** 31.

(14) Li, X.-Y.; Czernuszewicz, R. S.; Kincaid, J. R.; Spiro, T. G. *J. Am. Chem. Soc*. **1989**, *111*, 1**,** 7012.

(15) (a) Shelnutt, J. A.; Cheung, L. D.; Cheng, C. C.; Yu, N.-T.; Felton, R. H. *J. Chem. Phys.* **1977**, *66*, 3387. (b) Shelnutt, J. *J. Chem. Phys.* **1980**, *72*, 3948. Shelnutt, J. *J. Chem. Phys* **1981**, *74*, 6644.

(16) (a) Mou, C.; Chen, D.-M.; Wang, X.; Zhang, B.; He, T.; Liu, F.-C. *Chem. Phys. Lett.* **1991**, *179*, 237. (b) Mou, C.; Chen, D.-M.; Wang, X.; Zhang, B.; He, T.; Liu, F.-C. *Spectrochim. Acta* **1991**, *47*, 1575.

(17) (a) Zgierski, M.; Pawlikowski, M.; *Chem. Phys. Lett.* **1981**, *78*, 451. (b) Zgierski, M.; Shelnutt, J.; Pawlikowski, M. *Chem. Phys. Lett.* **1979**, *68*, 262.

(18) Rush, T., III; Kumble, R.; Spiro, T. G. *J. Phys. Chem.* **1996**, *100*, 12076.

(19) Kumble, R.; Rush, T., III; Blackwood, M. B.; Kozlowski, P. M.; Spiro, T. G. *J. Phys. Chem.* **1998**, *102*, 7280.

(20) Schick, G. A.; O'Grady, M. R.; Tiwari, R. K. *J. Phys. Chem.* **1993**, *97*, 1339.

(21) Pasternack, R. F.; Schaefer, K. F.; Hambright, P. *Inorg. Chem.* **1994**, *33*, 2062.

(22) Ribo, J. M.; Crusats, J.; Farrera, J.-A.; Valero, M. L. *J. Chem. Soc. Chem. Commun.* **1994**, 681.

(23) Ohno, O.; Kaizu, Y.; Kobayashi, H. *J. Chem. Phys.* **1993**, *99*, 4128.

(24) Akins, D. A.; Ozcelik, S.; Zhu, H. R.; Guo, C. *J. Phys. Chem.* **1996,** *100*, 5420; 14390.

(25) Guo, C.; Ren, B.; Akins, D. A.; *J. Phys. Chem.* **1998**, *102*, 8751.

(26) Chen, D.-M.; Li, X.-Y.; Yu, N.-T.; Zhang, Y.; He, T.; Liu, F.-C. *Chem. J. Chin. Univ.* **1999**, *20*, 1097.

(27) Adler, A. D. *J. Org. Chem.* **1967**, *32*, 2**,** 476.

(28) Busby, C. A. *Can. J. Chem.* **1975**, *35*, 5**,** 1554.

(29) (a) Akins, D. A. *J. Phys. Chem.* **1986**, *90*, 1530. (b) Akins, D. A.; Lombardi, J. R. *Chem. Phys. Lett.* **1987**, *135*, 495.

(30) Akins, D. A.; Akabli, C. K.; Li, X. *J. Phys. Chem.* **1989**, *93*, 1977.

(31) Kasha, M.; Rawls, H. R.; El-Baypomi, M. A. *Pure Appl. Chem.* **1965**, *11***,** 371.

(32) Spano, F. C. *Phys. Rev. Lett*. **1991**, *67*, 3424; *ibid* **1992**, *68*, 2976.

(33) Van Burgel, M.; Wiersma, D. A.; Duppen, K. *J. Chem. Phys*. **1995**, *102***,** 20.

(34) Knapp, E. W. *Chem. Phys.* **1984**, *85*, 73.

(35) The program used in the present work was adapted from a Fortran code provided by Prof. A. B. Myers on a workshop during the Fifteenth International Conference On Raman Spectroscopy (ICORS-15th, Pittsburgh, 1996).

(36) Stone, A.; Fleischer, E. B. *J. Am. Chem. Soc*. **1968**, *90*, 2735.

(37) Sparks, L. D.; Medforth, C. J.; Park, M.-S.; Chamberlain, J. R.; Ondrias, M. R.; Senge, M. O.; Smith, K. M.; Shelnutt, J. A. *J. Am. Chem. Soc.* **1993**, *115*, 581.

(38) Akins, D. A.; Macklin, J. W.; Parker, L. A.; Zhu, H.-R. *Chem. Phys. Lett*. **1990**, *169*, 564.

(39) Akins, D. L.; Ozcelik, S.; Zhu, H.-R.; Guo, C. *J. Phys. Chem.* **1997**, *101*, 1**,** 3251.

(40) Blazej, D. C.; Peticolas, W. L. *Proc. Natl. Acad. Sci. U.S.A.* **1977**, *74*, 2639.

(41) Fuhrhop, J.-H.; Demoulin, C.; Boettcher, C.; Koning, J.; Siggel, U. *J. Am. Chem. Soc*. **1992**, *114*, 4159.

(42) Schick, G. A.; Schreiman, I. C.; Wagner, R. W.; Lindsey, J. S.; Bocian, D. F. *J. Am. Chem. Soc*. **1989**, *111*, 1344.

(43) Czikkley, V.; Forstering, H. D., Kuhn, H. *Chem. Phys. Lett.* **1970**, *6*, 207.

(44) Hassing, S.; Mortensen, O. S. *J. Mol. Spectrosc.* **1981**, *87*, 1.